Check for updates

Received: 2 October 2020 | Revised: 7 December 2020 | Accepted: 9 December 2020

DOI: 10.1002/mrc.5122

SPECIAL ISSUE RESEARCH ARTICLE

WILEY

^{17}O solid-state NMR at ultrahigh magnetic field of 35.2 T: Resolution of inequivalent oxygen sites in different phases of MOF MIL-53(Al)

Vinicius Martins[1] | **Jun Xu**[2] | **Ivan Hung**[3] | **Zhehong Gan**[3] | **Christel Gervais**[4] | **Christian Bonhomme**[4] | **Yining Huang**[1]

[1]Department of Chemistry, The University of Western Ontario, London, ON, Canada

[2]Center for Rare Earth and Inorganic Functional Materials, Tianjin Key Lab for Rare Earth Materials and Applications, School of Materials Science and Engineering & National Institute for Advanced Materials, Nankai University, Tianjin, China

[3]National High Magnetic Field Laboratory (NHMFL), Tallahassee, FL, USA

[4]CNRS, UMR 7574, Laboratoire de Chimie de la Matière Condensée de Paris, LCMCP, Sorbonne Université, Paris, France

Correspondence
Yining Huang, Department of Chemistry, The University of Western Ontario, 1151 Richmond Street, London, ON N6A 5B7, Canada.
Email: yhuang@uwo.ca

Jun Xu, Center for Rare Earth and Inorganic Functional Materials, Tianjin Key Lab for Rare Earth Materials and Applications, School of Materials Science and Engineering & National Institute for Advanced Materials, Nankai University, Tianjin 300350, China.
Email: junxu@nankai.edu.cn

Funding information
Open Funds, Grant/Award Number: KF1818; National Natural Science Foundation of China, Grant/Award Number: 21904071 and 22071115

Abstract

MIL-53(Al) is a member of the most extensively studied metal–organic framework (MOF) families owing to its "flexible" framework and superior stability. ^{17}O solid-state NMR (SSNMR) spectroscopy is an ideal site-specific characterization tool as it probes local oxygen environments. Because oxygen local structure is often altered during phase change, ^{17}O SSNMR can be used to follow phase transitions. However, ^{17}O is a challenging nucleus to study via SSNMR due to its low sensitivity and resolution arising from the very low natural abundance of ^{17}O isotope and its quadrupolar nature. In this work, we describe that by using ^{17}O isotopic enrichment and performing ^{17}O SSNMR experiments at an ultrahigh magnetic field of 35.2 T, all chemically and crystallographically inequivalent oxygen sites in two representative MIL-53 (Al) (as-made and water adsorbed) phases can be completely resolved. The number of signals in each phase is consistent with that predicted from the space group refined from powder X-ray diffraction data. The ^{17}O 1D magic-angle spinning (MAS) and 2D triple-quantum MAS (3QMAS) spectra at 35.2 T furnish fine information about the host–guest interactions and the structural changes associated with phase transition. The ability to completely resolve multiple chemically and crystallographically inequivalent oxygen sites in MOFs at very high magnetic field, as illustrated in this work, significantly enhances the potential for using the NMR crystallography approach to determine crystal structures of new MOFs and verify the structures of existing MOFs obtained from refining powder X-ray diffraction data.

KEYWORDS

^{17}O, flexible MOFs, host–guest interaction, MIL-53(Al), NMR crystallography, phase transition, solid-state NMR spectroscopy

Vinicius Martins and Jun Xu contributed equally to this work.

 © 2020 John Wiley & Sons, Ltd.

1 | INTRODUCTION

Metal–organic frameworks (MOFs) are a class of inorganic–organic hybrid porous materials that have attracted tremendous attention in the last decades.[1] The remarkable variability and tunability of the composition, structure, and property of MOFs are the most striking characteristics, distinguishing themselves from other inorganic porous materials such as zeolites. Flexible MOFs are an important branch of MOF family. They can undergo reversible crystal-to-crystal phase transition upon external stimuli such as host–guest interactions and physical stimuli, resulting in drastic changes in unit cell volume and pore dimension.[2] The marked change in unit cell volume can be used for applications in sensors, switching devices, micromechanical devices, and so forth. Furthermore, the dynamic switching of MOF channels is ideal for selective adsorption of guest molecules.[2]

Perhaps, the most prominent member of flexible MOFs is MIL-53. Although many MOF systems exhibit some structural flexibility, the majority of current research is focused on the MIL-53 family due to their superior thermal (up to 500°C) and chemical (in water and many solvents) stability. The structural flexibility of MIL-53 is often demonstrated by the change in pore dimension during MOF activation and subsequent hydration (Figure 1).[3] By removing the residual linker precursor (1,4-benzenedicarboxylic acid, H_2BDC) molecules occluded inside the MOF channels during synthesis, the pore dimension of MIL-53(Al), a prototypical member of MIL-53, increases from 7.3 × 7.7 $Å^2$ in the as-made phase (i.e., MIL-53(Al)-*as*) to 8.5 × 8.5 $Å^2$ in the large-pore phase (i.e., MIL-53(Al)-*lp*). The large-pore phase can adsorb water to yield a narrow-pore phase (i.e., MIL-53 (Al)-*np*) with compressed channels of 2.6 × 13.6 $Å^2$. Despite the drastic changes in channel dimension accompanied by the change in crystal structure, the framework topology is retained during the phase transition. The main driving force for phase transition and dynamic switching of channel size is hydrogen bonding,[3,4] but other types of host–guest interactions such as π–π stacking and van der Waals forces are also considered to be factors.[5] These interactions are not only responsible for the structural changes but also play critical roles in their applications such as xylene separation.[6] Thus, a better understanding of the host–guest interactions in these systems through characterization of different phases are critically important for designing new flexible MOFs. The information on crystal structures of different phases associated with dynamic switching mainly come from the X-ray diffraction (XRD)-based methods. However, more often than not, guest molecules are disordered, and they undergo rapid thermal motions within MOF channels. Furthermore, the details of hydrogen bonding are usually unavailable due to the insensitivity of XRD to hydrogen atoms within the crystal structure.

Solid-state NMR (SSNMR) spectroscopy is a nuclide- and site-specific characterization tool complementary to XRD-based techniques.[7] It is sensitive to the changes in both long-range ordering upon phase transition and local environment induced by host–guest interactions. Previous SSNMR studies provided valuable information on host–guest interaction and structural change associated with phase transitions in MIL-53(Al).[1,4,5] The mechanism of dynamic switching during MOF activation and hydration was first rationalized on the basis of ^{1}H, ^{13}C, and ^{27}Al SSNMR data.[1,4,5] The adsorption of xylene isomers, aromatic compounds, and nitrogen bases was further examined by ^{1}H, ^{13}C, ^{27}Al, and ^{2}H SSNMR experiments.[5c–h] A ^{129}Xe SSNMR study also illustrated that the large-pore to narrow-pore transformation can be triggered by weak van der Waals forces between xenon atoms and the framework.[5i]

Oxygen is a key constituent of MIL-53(Al). It exists in two different species within the framework: the carboxylate group ($-COO^-$), and the μ_2-hydroxyl group bridging two AlO_6 octahedra (Al–OH–Al). These two oxygen-containing functional groups play prominent roles in the

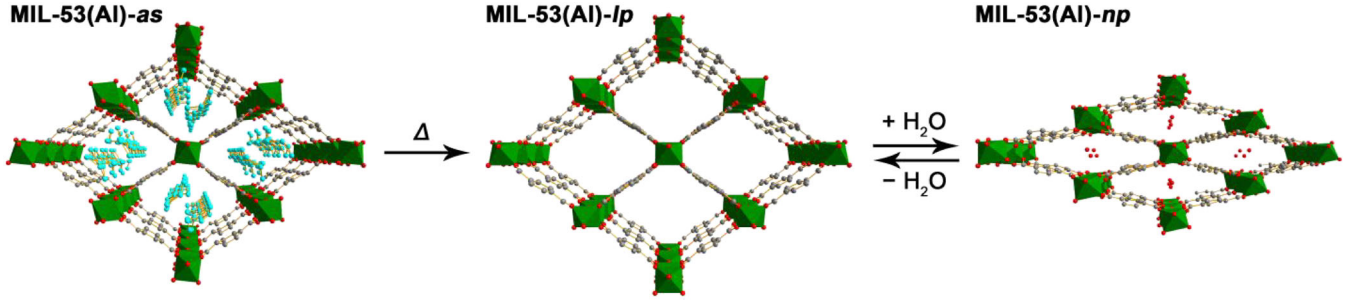

FIGURE 1 Schematic illustrations of the transformation between three MIL-53(Al) phases. Color coding: Al, green; O, red; C, grey; H_2BDC, turquoise. The hydrogen atoms are omitted for clarity

phase transition associated with the breathing of MIL-53 (Al) and are directly involved in host–guest interactions such as hydrogen bonding.[4] ^{17}O SSNMR spectroscopy should be ideal for probing phase transitions of MIL-53 (Al) that alter the geometric and electronic environments of oxygen as ^{17}O is highly sensitive to both the chemical shift (CS) and quadrupolar interactions.[8] However, ^{17}O SSNMR is, in general, more challenging than ^{1}H, ^{13}C, and ^{27}Al SSNMR, due to the fact that ^{17}O has extremely low natural abundance (0.038%) and a relatively low gyromagnetic ratio ($\gamma = -5.774$ MHz T^{-1}), although high-resolution proton SSNMR can be challenging as well, but for a different reason. Furthermore, ^{17}O (spin $I = 5/2$) is quadrupolar[9] and, therefore, often suffers from the line broadening induced by the second-order quadrupolar interaction. ^{17}O isotopic enrichment can dramatically increase the sensitivity.[10] Performing ^{17}O SSNMR experiments at high magnetic fields (≥18.8 T) can significantly improve spectral resolution (as the second-order quadrupolar interaction in frequency is inversely proportional to the strength of magnetic field) and enhances the sensitivity as well.

^{17}O SSNMR has been employed to examine the MIL-53 MOFs. Ashbrook et al. studied the mixed-metal MIL-53(Al and Ga) at 14.1 and 20.0 T. The results provide valuable information on the final composition of the materials, the preference for cation clustering/ordering within the MOFs, and the unusual breathing behavior.[10e,f] Previously, we also acquired ^{17}O SSNMR spectra of MIL-53(Al)-*as* and MIL-53(Al)-*np* at 21.1 T.[10d] Although significant differences in ^{17}O spectra were observed between the two phases, the multiple crystallographically inequivalent carboxylate oxygen sites in each phase were not resolved.

Very recently, we demonstrated that very high ^{17}O spectral resolution can be achieved for MOF systems at ultrahigh magnetic field of 35.2 T.[11] In the abovementioned reference, we examined the effect of activation on the MIL-53(Al) framework oxygen. At this highest magnetic field available to chemists today,[12] significantly higher spectral resolution and sensitivity achieved allowed us to distinguish partially activated from completely activated MIL-53(Al) (note: the completely activated MIL-53(Al) corresponds to MIL-53 (Al)-*lp* phase) and resolve multiple oxygen environments in partially-activated MIL-53(Al). Encouraged by this work, we further carried out an ^{17}O SSNMR study of MIL-53(Al) at 35.2 T. The high spectral resolution and sensitivity at this field permit every inequivalent oxygen site to be differentiated in the MIL-53(Al)-*as* and MIL-53 (Al)-*np* phases. Both the electric field gradient (EFG) and chemical shift (CS) tensor values for each oxygen site were also extracted.

2 | EXPERIMENTAL METHODS

2.1 | Sample preparation

The MIL-53(Al)-*as* sample was synthesized by the dry gel conversion method described in our previous work.[10d] All starting materials were used as received without further purification. A mixture of Al $(NO_3)_3{\cdot}9H_2O$ (1.6880 g or 4.5 mmol) and 1,4-benzenedicarboxylic acid (H_2BDC, 0.9802 g or 5.9 mmol) was placed in a 23 ml of Teflon-lined autoclave charged with 0.5 ml of ^{17}O-enriched water (CortecNet, 35 atom %), see Scheme S1 for the reaction vessel. The autoclave was sealed and heated in an oven at 220°C for 3 days. After slowly cooling to room temperature, MIL-53(Al)-*as* was collected as a white powder under vacuum filtration, washed with DMF, and dried in the air at 80°C. MIL-53(Al)-*lp* was prepared by first solvent exchanging MIL-53(Al)-*as* with DMF for 24 h and then activating it at 300°C under dynamic vacuum for 12 h. MIL-53(Al)-*np* was obtained by exposing MIL-53(Al)-*lp* to air overnight. The phase purity and crystallinity of ^{17}O-enriched samples were confirmed by powder XRD patterns (Figure S1). The degree of ^{17}O exchange is about 5.8% as the abovementioned samples were prepared under exactly the same conditions as those described in He et al.[10d]

2.2 | SSNMR spectroscopy

^{17}O SSNMR experiments were conducted at 35.2 T on a series-connected hybrid (SCH) magnet (^{17}O Larmor frequency: 203.4 MHz) at the National High Magnetic Field Laboratory (NHMFL) in Tallahassee, USA.[12b] A Bruker Avance NEO console and a 3.2 mm of MAS probe designed and built at the NHMFL were used. The MAS rate was 18 kHz. Because this probe is a single-resonance probe, consequently, the spectra are not ^{1}H-decoupled. However, because the focal point of this paper is to resolve inequivalent carboxylate oxygen sites, it should be pointed out that the ^{1}H–^{17}O dipolar coupling for the carboxylate oxygen in this MOF is relatively weak. In fact, the magnitude of the dipolar coupling between a carboxylate oxygen and a nearby phenyl proton is only about 1 kHz. Furthermore, our previous experience with similar compounds at lower fields indicates that ^{1}H decoupling does not improve the resolution of carboxylate oxygen drastically.

A pulse delay of 0.1 s was used, which was preoptimized to achieve the highest signal-to-noise (S/N) ratio. When different pulse delays were used, the observed NMR lineshapes did not exhibit significant changes. ^{17}O 1D MAS NMR spectrum of MIL-53(Al)-*as*

was acquired by using a rotor-synchronized spin echo sequence with a 90° pulse of 2 μs and an interpulse delay of one rotor period. ^{17}O 1D MAS NMR spectrum of MIL-53(Al)-*lp* was acquired by using a one-pulse sequence with a 90° pulse of 2 μs. ^{17}O 1D MAS NMR spectrum of MIL-53(Al)-*np* was acquired by using a rotor-synchronized spin-echo sequence with a 90° pulse of 5 μs and an interpulse delay of 10 rotor periods for a whole spin-echo signal. ^{17}O 2D rotor-synchronized shifted-echo triple-quantum MAS (3QMAS) spectra were measured by using 3Q excitation and conversion pulses of 3.75 and 1.25 μs, respectively. 2D 3QMAS spectra were processed with the *Q*-shearing procedure using the MATLAB script (MathWorks Inc.) described in Hung et al.[13] In general, the choice of a pulse length(s) for a particular experiment is based on the trade-off between the bandwidth and central transition (CT)-selectivity for sites with small C_Q values. Therefore, selection of a pulse length was made during the experimental optimization.

All ^{17}O NMR spectra were referenced to liquid water at 0 ppm. More NMR experimental details can be found in Tables S1 and S2.

2.3 | Spectral simulations

The strong interaction between the electric quadrupole moment of ^{17}O ($I = 5/2$) and the surrounding EFG yields broad powder patterns rather than sharper resonances. Enhanced at high magnetic fields such as 35.2 T, the CS interaction interplays with the quadrupolar interaction, making the lineshape of powder patterns more complicated and difficult to simulate. The dmfit software package was used to simulate ^{17}O SSNMR spectra using the Int2QUAD mode, taking both the quadrupolar and the CS effects into consideration.[14] The EFG tensor is described in dmfit by using three principal components in the following order:$|V_{YY}| \leq |V_{XX}| \leq |V_{ZZ}|$. The quadrupolar coupling constant (C_Q) and asymmetry parameter (η_Q) are defined as follow: $C_Q = (eQV_{ZZ}/h) \times 9.7177 \times 10^{21}$ (in Hz) and $\eta_Q = (V_{YY} - V_{XX})/V_{ZZ}$, where e is the electric charge, Q is the quadrupole moment (-2.558×10^{-30} m^2),[9] and a conversion factor of 9.7177×10^{21} V m^{-2} is used to convert C_Q from atomic units to Hz. C_Q and η_Q describe the spherical and cylindrical symmetry of the EFG tensor, respectively. The CS tensor is described by three principal components such that $|\delta_{22} - \delta_{iso}| \leq |\delta_{11} - \delta_{iso}| \leq |\delta_{33} - \delta_{iso}|$. The isotropic CS $\delta_{iso} = (\delta_{11} + \delta_{22} + \delta_{33})/3$, and two chemical shift anisotropy (CSA) parameters are defined by $\Delta_{CS} = \delta_{33} - \delta_{iso}$ and $\eta_{CS} = |(\delta_{22} - \delta_{11})/\Delta_{CS}|$. Three Euler angles ($\varphi$, χ, and ψ) describe the orientations of the CS tensor with respect to the EFG principal axis frame. As a result, eight independent parameters, C_Q, η_Q, δ_{iso}, Δ_{CS}, η_{CS}, φ, χ, and ψ, are required to characterize a single ^{17}O site when both the quadrupolar and CSA effects are considered. Only the center transition ($+1/2 \leftrightarrow -1/2$) was considered in spectral simulations of the ^{17}O 1D MAS spectra of MIL-53(Al)-*np* and MIL-53(Al)-*as*. For MIL-53(Al)-*lp*, the spinning sideband (SSB) pattern suggests the observation of satellite transitions. Therefore, the $+3/2 \leftrightarrow +1/2$ and $-1/2 \leftrightarrow -3/2$ transitions were also included to reproduce the SSBs of the 1D MAS spectrum. Seeing the satellite transitions is likely due to the hard 90° excitation pulse used.[15] All uncertainties in NMR parameters were estimated by variation of the parameter of interest in both directions from the best-fit value while holding all other NMR parameters constant.

2.4 | Theoretical calculations

Input unit cell parameters and atomic coordinates of three MIL-53(Al) phases were taken from the reference.[4] Due to the disordered nature of H_2BDC in channels of MIL-53(Al)-*as*, they were removed prior to periodic density functional theory (DFT) calculations. The missing H atoms of BDC^{2-} linkers, μ_2-hydroxyl group, and water molecules in MIL-53(Al)-*np* were initially positioned to be consistent with the expected structure of the system and all atomic positions were then relaxed with the Vienna Ab-initio Simulation Package (VASP) code,[16] keeping fixed unit cell parameters set to the XRD parameters. The NMR parameters were then calculated by using the QUANTUM-ESPRESSO code,[17] keeping the atomic positions equal to the values previously calculated with VASP. The Gauge-including Projector Augmented Wave (GIPAW) approach involved in QUANTUM-ESPRESSO enables the reproduction of the results of a fully converged all-electron calculation.[18] Calculations were performed using the generalized gradient approximation (GGA) with Perdew, Burke, and Ernerhof (PBE) functionals and norm-conserving pseudopotentials,[19] in the Kleinman–Bylander form.[20] The wave functions are expanded on a plane-wave basis set with a kinetic energy cut-off of 80 Ry. For the charge density and CS tensor calculation, the integrals over the first Brillouin zone are performed using Monkhorst–Pack grids of $1 \times 3 \times 1$, $3 \times 1 \times 1$, and $1 \times 3 \times 3$ *k*-points for MIL-53(Al)-*as*, MIL-53(Al)-*lp*, and MIL-53(Al)-*np*, respectively. The isotropic chemical shift δ_{iso} is defined as $\delta_{iso} = \sigma_{iso}$ (ref) $- \sigma_{iso}$, where σ_{iso} (ref) is the isotropic chemical shielding of the same nucleus in a reference system. In the present case, the comparison between the experimental ^{17}O δ_{iso} and calculated σ_{iso} values for Na_2SiO_3, α-$Na_2Si_2O_5$, α- and γ-glycine, and α-$SrSiO_3$

enabled the determination of the relation between δ_{iso} and calculated σ_{iso} values for the ^{17}O nucleus as previously described.[10c]

3 | RESULTS AND DISCUSSION

The framework of MIL-53(Al) is composed of unidimensional chains of μ_2-OH-bridged $AlO_4(OH)_2$ octahedra interconnected by BDC^{2-} linkers, exhibiting 1D rhombic channels. Although the framework topology is retained during the dynamic switching of the structure, the crystal symmetry indeed varies from orthorhombic *Pnma* (#62) for MIL-53(Al)-*as*, to orthorhombic *Imma* (#72) for MIL-53(Al)-*lp*, to eventual monoclinic *Cc* (#9) for MIL-53(Al)-*np*, respectively.[4] There is only one μ_2-OH oxygen site present in all three phases. The number of inequivalent $-COO^-$ oxygen sites, however, varies, depending on the crystal symmetry. Specifically, the numbers of $-COO^-$ oxygen sites are 2, 1, and 4 for MIL-53(Al)-*as*, MIL-53(Al)-*lp*, and MIL-53(Al)-*np*, respectively (Figure 2).

As mentioned earlier, ^{17}O SSNMR experiments of MIL-53(Al)-*as* and MIL-53(Al)-*np* were previously performed at magnetic fields lower than 35.2 T.[10d–f] Figure 2 shows ^{17}O 1D MAS spectra of MIL-53(Al)-*as* and MIL-53(Al)-*np* at 21.1 T.[10d] Two ^{17}O spectral envelopes corresponding to $-COO^-$ (~220 ppm) and μ_2-OH (~20 ppm) oxygen sites are seen in the 1D MAS spectrum of MIL-53(Al)-*as*. For MIL-53(Al)-*np*, three signals including two in the $-COO^-$ and one in the μ_2-OH oxygen regions were identified. However, the number of observed $-COO^-$ signals for each phase is only half of what is expected from the crystal symmetry, implying that not all inequivalent $-COO^-$ oxygen sites were resolved at this field.

As reported in the recent literature,[11,12] performing ^{17}O SSNMR measurements at the highest accessible magnetic field strength can drastically enhance both spectral sensitivity and resolution. Therefore, in the present study, we acquired ^{17}O 1D MAS spectra of two MIL-53(Al) phases at 35.2 T (Figure 2). At this ultrahigh magnetic field, the signals of both MIL-53(Al)-*as* and MIL-53(Al)-*np* phases become considerably narrower due to the reduction of the second order quadrupolar broadening. At 35.2 T, the SSBs are significantly enhanced, especially for the $-COO^-$ oxygen, indicating the drastically amplified CSA in frequency by the high field. The ^{17}O

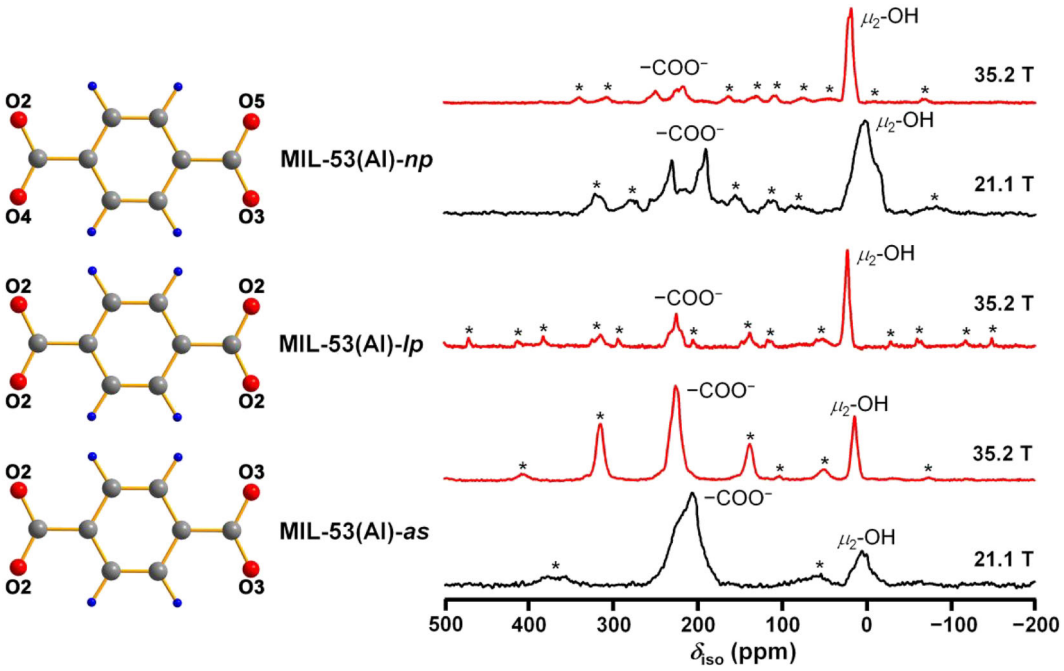

FIGURE 2 Left: The inequivalent $-COO^-$ oxygen sites in different phases. Color coding: O, red; C, grey; H, blue. Right: ^{17}O 1D MAS NMR spectra of ^{17}O-enriched MIL-53(Al) samples at 35.2 T (red) and 21.1 T (black). MIL-53(Al)-*as*: the top two spectra; MIL-53(Al)-*lp*: the middle spectrum; MIL-53(Al)-*np*: the bottom two spectra. The asterisk (*) denotes spinning sidebands (SSBs). The ^{17}O 1D MAS NMR spectra of MIL-53(Al)-*as* and MIL-53(Al)-*np* at 21.1 T, and the ^{17}O spectrum of MIL-53(Al)-*lp* at 35.2 T are adapted with permission from the American Chemical Society.[10d,11] Note: the numbers of transients accumulated for each spectrum at 35.2 T were only 1/4 and 1/8 of those at 21.1 T for MIL-53(Al)-*as* and MIL-53(Al)-*np*, respectively. The sample volume (~36 μl) at 35.2 T was less than half of that (~80 μl) at 21.1 T

spectrum of MIL-53(Al)-*lp* at 35.2 T was recently published.[11] For comparison, it is also included in Figure 2.

Although ^{17}O signals in the 1D MAS spectra become considerably narrower at 35.2 T, the number of $-COO^-$ oxygen signals for MIL-53(Al)-*as* and MIL-53(Al)-*np* remains the same as seen at 21.1 T, suggesting that even at 35.2 T, the maximum achievable ^{17}O spectral resolution in 1D MAS experiments is still insufficient to resolve all inequivalent oxygen sites. This is because some sites have very similar local environments and simply spinning the sample at the magic angle cannot completely average out the second-order quadrupolar interaction. To achieve higher spectral resolution, we have carried out ^{17}O 3QMAS experiments,[21] as this technique can completely eliminate the second-order quadrupolar broadening along the indirect F1 dimension and therefore should separate the overlapping signals in the 1D MAS spectrum. Figure 3 illustrates the 3QMAS spectra of MIL-53(Al)-*np* and MIL-53(Al)-*as* in the carboxylate oxygen region. Higher spectral resolution was indeed achieved as four and two $-COO^-$ oxygen sites are resolved along the F1 dimension of the spectra of MIL-53 (Al)-*np* and MIL-53(Al)-*as*, respectively. For both phases, the number of inequivalent $-COO^-$ oxygen sites seen in the 3QMAS spectra is now consistent with that predicted by the crystal structures.[4] It should be mentioned that the 3QMAS experiment was also carried out at 21.1 T. However, after 21 h of acquisition, the two inequivalent carboxylate oxygen sites of MIL-53(Al)-as were not resolved in the 3QMAS spectrum (Figure S2) at this field.

Analyzing 3QMAS spectra yields the quadrupolar parameters for each oxygen site. For each resolved ^{17}O signal along the F1 dimension, the corresponding F2 cross-section can be extracted at δ_1 (in ppm). The δ_1 and the spectral center of gravity (δ_2, in ppm) along the F2 dimension can be used to calculate the isotropic chemical

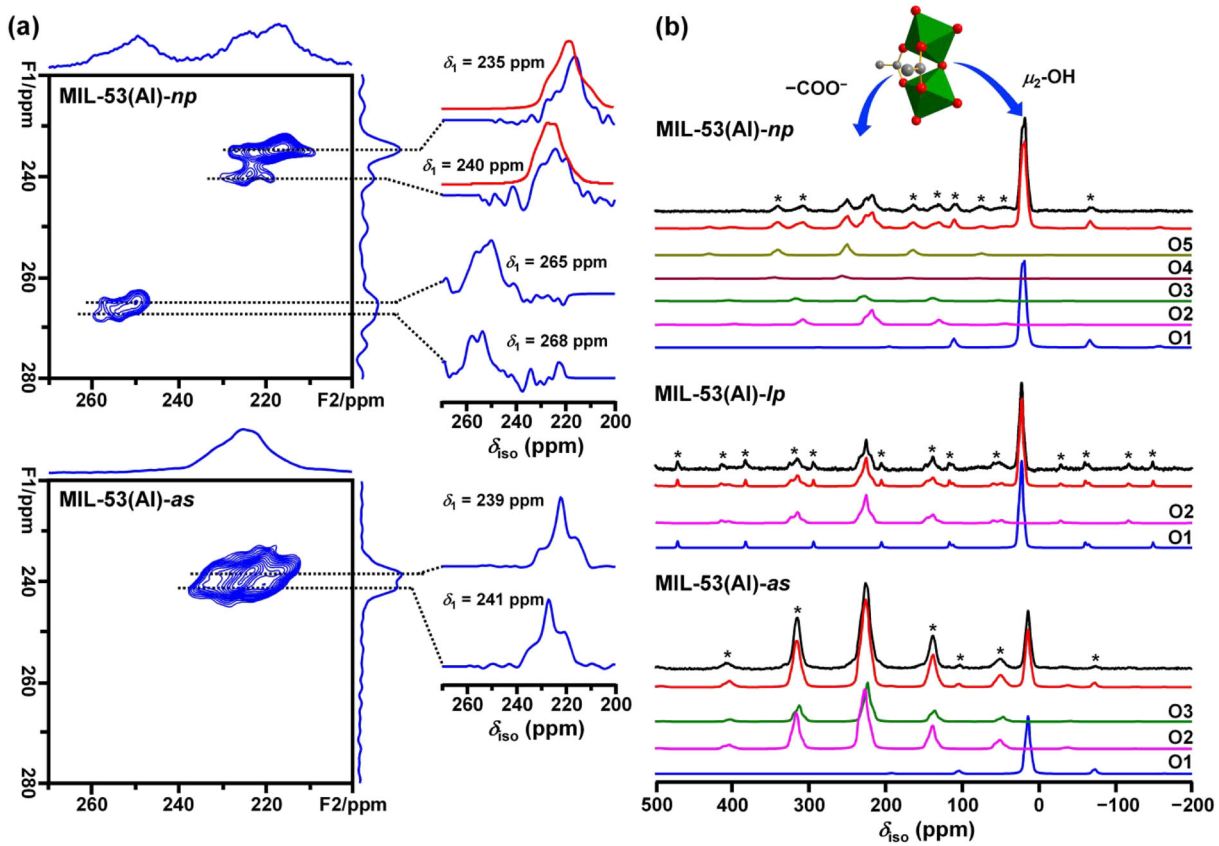

FIGURE 3 (a) ^{17}O 2D 3QMAS NMR spectra of ^{17}O-enriched MIL-53(Al)-*as* and MIL-53(Al)-*np* at 35.2 T. Black dashed lines correspond to the slices extracted for analyses. Blue and red solid lines denote experimental and simulated spectra, respectively. Only the regions corresponding to $-COO^-$ oxygen sites are shown for clarity. The 3QMAS spectra were acquired using a shifted-echo MQMAS pulse sequence and rotor synchronized t_1 and processed using the Q-shearing method to avoid spectral folding of the peaks and spinning sidebands (SSBs).[13] The total experimental times are 1.3 and 3.4 h for MIL-53(Al)-*as* and MIL-53(Al)-*np*, respectively. (b) Experimental and simulated ^{17}O 1D MAS NMR spectra of three MIL-53(Al) phases at 35.2 T. Both the quadrupolar and CSA effects are considered in simulation by using the parameters shown in Table 1. Asterisks (*) denote SSBs. The two oxygen species in MIL-53(Al) were shown on the top. The ^{17}O spectrum of MIL-53(Al)-*lp* at 35.2 T is adapted with permission from the American Chemical Society[11]

shift δ_{iso} (in ppm) and the quadrupolar product, $P_Q = C_Q(1 + \eta_Q^2/3)^{1/2}$ (in MHz) using the following equations[10e,f,22]:

$$\delta_{iso} = \frac{17}{27}\delta_1 + \frac{10}{27}\delta_2,$$

$$P_Q = \left\{\frac{170}{81}\frac{[4I(2I-1)]^2}{[4I(I+1)-3]}(\delta_1 - \delta_2)\right\}^{1/2} \cdot \nu_0 \times 10^{-3},$$

where ν_0 is the Larmor frequency (in MHz) and I is the spin quantum number.

The extracted δ_{iso} and P_Q values of each $-COO^-$ oxygen site of MIL-53(Al)-*as* and MIL-53(Al)-*np* are shown in Table S3. The values of these two parameters were determined directly from the resonance positions along F1 and F2 dimensions and do not require accurate lineshape fitting along the F2 dimension.

To assign the observed ^{17}O NMR signals to crystallographic $-COO^-$ oxygen sites, the δ_{iso} values of each inequivalent oxygen site were predicted by the GIPAW DFT calculations under periodic boundary conditions (Table S4). It has been well established that although the calculated δ_{iso} values may not exactly match the experimental δ_{iso} values, assignments of multiple signals based on relative calculated δ_{iso} values are valid.[8h,10b,c,11,23] A comparison between calculated and experimental δ_{iso} values permits individual assignment of $-COO^-$ oxygen signals. For instance, the calculated δ_{iso} values of $-COO^-$ oxygen sites are ordered O4 > O5 > O3 > O2 for MIL-53(Al)-*np*. The ^{17}O signal with the highest δ_{iso} of 264 ppm is, therefore, assigned to O4, the ^{17}O signal with the second-highest δ_{iso} of 260 ppm is assigned to O5 and so forth. The two $-COO^-$ oxygen signals of MIL-53(Al)-*as* are assigned similarly.

For MIL-53(Al)-*np*, O2 and O3 signals are well resolved in the F2 dimension, and their line-shapes along F2 cross-section are also well defined. Their C_Q, η_Q, and δ_{iso} values can be extracted by fitting the F2 cross-sections (Table S3), and they were used as initial inputs to simulate the 1D MAS spectra for final refinement. However, the signals of O4 and O5 sites overlap, and the lineshapes of their F2 cross-sections are not well-defined. For these two sites, using experimentally obtained P_Q and theoretically calculated η_Q, we derived their C_Q values according to their relationship of $P_Q = C_Q(1 + \eta_Q^2/3)^{1/2}$. The C_Q, η_Q, and δ_{iso} values were further refined by simulating the 1D MAS spectra. MIL-53(Al)-*np* has five oxygen sites including the μ_2-OH oxygen. Forty parameters in total are required if both the EFG and CSA effects are considered. To reduce the number of parameters, we first simulated the 1D MAS spectrum by only considering the quadrupolar interaction. We have demonstrated previously that at such a high magnetic field of 35.2 T, the EFG anisotropy of a carboxylate oxygen is much smaller than that of the CSA. The EFG is the primary source of line broadening for isotropic peaks, but only makes little contribution to the SSBs.[11] Indeed, the isotropic region in the simulated spectrum where only the effect of the EFG is considered matches well with the experimental spectrum (Figure S3), but the SSBs are negligible as expected. Figure S4 further illustrates an excellent agreement between experimental spectrum of MIL-53(Al)-*lp* and the simulated one where only the quadrupolar effect is considered, demonstrating that the main source of experimental resonance broadening of the isotropic peaks is the second-order quadrupolar interaction.

To reproduce the SSBs and obtain the CS tensor parameters, we further simulated the 1D spectrum by taking both the EFG and CSA effects into account. Specifically, five additional parameters are incorporated in the simulation: two CSA parameters including the reduced anisotropy Δ_{CS} and the CS asymmetry parameter η_{CS}, as well as three Euler angles (φ, χ, and ψ) describing the orientations of the CS tensor with respect to the EFG tensor principle axis frame.[14] The calculated Δ_{CS}, η_{CS}, and three Euler angles (φ, χ, and ψ) (Table S4) along with the C_Q, η_Q, and δ_{iso} values optimized in the previous steps were used as initial inputs for fitting the 1D MAS spectra. The final simulation allows us to refine and determine the final values of the eight parameters describing the EFG and CSA effects for each oxygen site. The final refined NMR parameters are summarized in Table 1.

The ^{17}O C_Q, η_Q, and δ_{iso} values of some oxygen sites in MIL-53(Al) were reported previously.[10d,e] However, because the experiments were conducted at the magnetic fields at 21.1 T or lower, the lower sensitivity and resolution did not allow all inequivalent $-COO^-$ oxygen sites to be resolved. In the present study, we were able to resolve all inequivalent oxygen sites of MIL-53(Al)-*as* and MIL-53(Al)-*np* phases and extract ^{17}O C_Q, η_Q, and δ_{iso} values for every site. It should be pointed out that the resolution of all inequivalent sites results from not only the high spectral resolution achieved at 35.2 T but also the significant boost to the sensitivity at this field. The high sensitivity gained at the ultrahigh field has made the ^{17}O 3QMAS experiments performed in this study practically possible in just a matter of hours, not days. Such a gain in sensitivity is very significant, considering the ^{17}O-enriched MOFs used in this work were prepared by using only 35% ^{17}O-enriched water. Furthermore, this is the first time that the CSA parameters and Euler angles are reported for oxygen sites in various MIL-53 (Al) phases.

TABLE 1 Refined experimental ^{17}O NMR parameters of three MIL-53(Al) phases

Sample	Site	P_Q (MHz)	C_Q (MHz)	η_Q	δ_{iso} (ppm)	Δ_{CS} (ppm)	η_{CS}	φ (°)	χ (°)	ψ (°)
MIL-53(Al)-*as*	O1 (μ_2-OH)		5.78	0.75	19.6	94	0.22	90	0	0
	O2 ($-COO^-$)	8.6	7.41	0.74	236.4	−210	0.37	250	80	70
	O3 ($-COO^-$)	8.1	6.95	0.84	232.1	−184	0.63	180	85	40
MIL-53(Al)-*lp*	O1 (μ_2-OH)		5.42	0.72	27.4	65	0.72	90	0	0
	O2 ($-COO^-$)		7.45	0.81	235.8	−182	0.82	170	80	45
MIL-53(Al)-*np*	O1 (μ_2-OH)		6.37	0.50	25.6	−70	0.30	270	0	0
	O2 ($-COO^-$)	8.3	7.77	0.75	228.0	−182	0.72	140	90	80
	O3 ($-COO^-$)	8.1	7.36	0.55	235.0	202	0.95	280	45	160
	O4 ($-COO^-$)	7.5	6.95	0.63	258.0	−201	0.98	170	85	40
	O5 ($-COO^-$)	8.1	7.57	0.64	264.6	−182	0.54	80	40	260

Note: The estimated uncertainties are 0.5 MHz for P_Q, 0.05 MHz for C_Q, 0.05 for η_Q, 0.5 ppm for δ_{iso}, 10 ppm for δ_{CS}, 0.10 for η_{CS}, and 10° for φ, χ, and ψ, respectively.

In the present work, ^{17}O 2D 3QMAS experiments at an ultrahigh field of 35.2 T allow us to separate all inequivalent $-COO^-$ oxygen sites in both MIL-53(Al)-*as* and MIL-53(Al)-*np*. We previously also reported the ^{17}O MAS spectrum of MIL-53(Al)-*lp* at 35.2 T. Taken together, we have been able to unambiguously identify all chemically and crystallographically inequivalent oxygen sites in all three representative phases of MIL-53 (Al) at 35.2 T. The total number of resolved ^{17}O signals now matches the number of inequivalent oxygen sites expected from their crystal symmetry: three for MIL-53 (Al)-*as*, two for MIL-53(Al)-*lp*, and five for MIL-53 (Al)-*np*.[4] The experimental C_Q, η_Q, and δ_{iso} values of $-COO^-$ oxygen sites range from 6.95 to 7.77 MHz, 0.55 to 0.84, and 228.0 to 264.6 ppm, respectively, and these ranges are from 5.42 to 6.37 MHz, 0.50 to 0.75, and 19.6 to 27.4 ppm for μ_2-OH oxygen sites. Moreover, the magnitudes of the CSA of μ_2-OH oxygen sites ($|\Delta_{CS}|$: 65 to 94 ppm) are smaller than those of $-COO^-$ oxygen sites ($|\Delta_{CS}|$: 176 to 198 ppm), consistent with the literature.[8b]

At this point, it is informative to compare the ^{17}O NMR results obtained at 35.2 T with the information extracted from ^1H, ^{13}C, and ^{27}Al MAS NMR data.[1,4,5b,e,10e,f] In all cases, the changes in NMR spectra have been observed upon the transformation among three MIL-53 (Al) phases shown in Figure 1. ^1H MAS NMR is sensitive to the existence and identity of guest molecules within MOF channels.[1,4,10e,f] As a result, the ^1H MAS NMR spectrum of MIL-53(Al)-*as* looks distinctly different from that of MIL-53(Al)-*lp*. The ^{13}C cross-polarization (CP) MAS NMR spectra are particularly sensitive to the changes in local electronic environment around carboxylate groups induced by hydrogen bonding.[4,5b,10e,f] Consequently, the phase transition from MIL-53(Al)-*lp* to MIL-53(Al)-*np* induced by water adsorption is accompanied by a relatively large chemical shift of carboxylate carbon from 170 to 174 ppm.[4] The changes in the ^{27}Al MAS NMR spectra directly reflect the degree of distortion in $AlO_4(OH)_2$ octahedra during the phase transition.[4,5e] ^{27}Al NMR spectra are particularly sensitive to the phase change between MIL-53(Al)-*lp* and MIL-53(Al)-*np* as the C_Q value increases substantially from 8.4 to 10.67 MHz upon adsorption of water.

^{17}O SSNMR can also provide valuable information on structure, phase transition, and host–guest interaction in MIL-53. The chemical shift of the μ_2-OH oxygen is sensitive to the nature of metals that it bridges in the framework and has been used to confirm and quantify the incorporation of the second framework metal into mixed-metal MIL-53.[10e,f] The current and previous work has shown that ^{17}O SSNMR also has the ability to detect the two phase transitions in MIL-53(Al) involving three phases as shown in Figure 1. At 35.2 T, upon activation, MIL-53(Al)-*as* with the *Pnma* structure transforms to MIL-53(Al)-*lp* with the *Imma* structure, which coincides with a significant change in ^{17}O δ_{iso} of the μ_2-OH signal from 19.6 to 27.4 ppm (Figure 4). The μ_2-OH group is involved in the hydrogen bonding with the occluded linker precursor, H_2BDC, in MIL-53(Al)-*as*. This interaction is responsible for the slightly reduced channel dimension of MIL-53(Al)-*as* (7.3×7.7 Å^2) compared with MIL-53(Al)-*lp* (8.5×8.5 Å^2). Apparently, the significant change in isotropic chemical shift observed upon phase transition is due to the removal of hydrogen bonding interaction by activation. Adsorption of water induces the phase transformation from the MIL-53(Al)-*lp* to MIL-53(Al)-*np* phases. It is known that the μ_2-OH group is not directly involved in hydrogen bonding with water molecules because its ^1H chemical shift does not change upon water adsorption.[4] Consequently, the change in

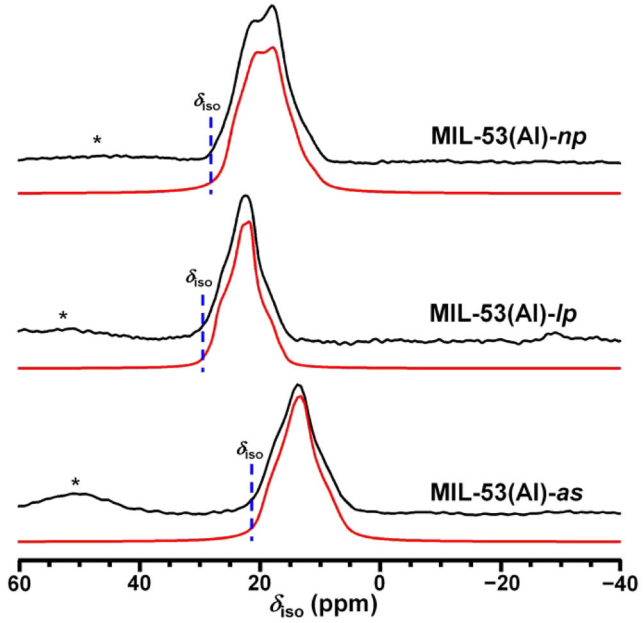

FIGURE 4 ^{17}O 1D experimental (black) and simulated (red) MAS NMR spectra of ^{17}O-enriched MIL-53(Al) samples at 35.2 T. blue dashed lines denote the isotropic chemical shift δ_{iso}. Only the regions corresponding to μ_2-OH oxygen sites are shown for clarity. Asterisks (*) denote SSBs. The ^{17}O spectrum of MIL-53(Al)-*lp* at 35.2 T is adapted with permission from the American Chemical Society[11]

the ^{17}O δ_{iso} value of μ_2-OH oxygen from MIL-53(Al)-*lp* to MIL-53(Al)-*np* is subtle. However, the changes in the ^{17}O C_Q (from 5.42 to 6.37 MHz) and η_Q (from 0.72 to 0.50) values are noticeable. The CSA parameters of μ_2-OH oxygen also alters upon water adsorption (Δ_{CS}: 65 to −70 ppm; η_{CS}: 0.72 to 0.30). These observations indicate that the adsorbed water molecules have induced observable differences in local environment of μ_2-OH, even when hydrogen bonds are not formed.

The phase transformation from MIL-53(Al)-*lp* to MIL-53(Al)-*np* upon water adsorption is evidenced from the significant change in the $-COO^-$ oxygen region of the ^{17}O 1D MAS spectra. Specifically, the splitting of the single $-COO^-$ oxygen peak in MIL-53(Al)-*lp* into two signals in the spectrum of MIL-53(Al)-*np* was observed at 35.2 T and lower fields.[10d–f] Ashbrook et al identified the signal with lower δ_{iso} value to the $-COO^-$ oxygen interacting with water via hydrogen bonding and the one at higher δ_{iso} value to the $-COO^-$ oxygen uninvolved in hydrogen bonding.[10e] The 3QMAS spectrum acquired at 35.2 T further illustrates that each $-COO^-$ oxygen signal seen in the 1D MAS spectrum actually originates from two overlapping signals. The peak with lower chemical shift results from the overlapping of O2 and O3 signals, whereas the higher chemical shift envelop is due to O4 and O5. Crystal structure indicates that the local environments of O2 and O3 are very similar as the bond lengths and angles involving the two oxygen sites are almost identical.[4] The same is true for O4 and O5. At 35.2 T, each pair of crystallographically inequivalent carboxylate oxygen with very similar local structures can be well distinguished, demonstrating that the very high ^{17}O spectral resolution and sensitivity achieved at this ultrahigh magnetic field permit one to differentiate oxygen sites with subtle differences in local geometry. The fact that the ^{17}O isotropic chemical shift values of O4 and O5 differ significantly from O2 and O3 upon adsorption of water confirms the previous results that only half of the $-COO^-$ oxygen sites are involved in the hydrogen bonding with water in MIL-53(Al)-*np*.[1,10e] As mentioned earlier, water adsorption indeed induces a shift of $-COO^-$ carbon towards the deshielded direction.[4] However, in each carboxylate group, one oxygen is directly involved in hydrogen bonding and the other is not, consequently, the impact of hydrogen bonding with water on each carboxylate carbon is the same. Therefore, the ^{13}C SSNMR data cannot pinpoint exactly which $-COO^-$ oxygen site participates in the hydrogen bonding.[4]

4 | CONCLUSIONS

In summary, the high ^{17}O spectral resolution and sensitivity achieved at 35.2 T (the highest magnetic field accessible to chemists to date) combined with 2D 3QMAS technique make it possible to resolve all inequivalent $-COO^-$ oxygen sites in three MIL-53(Al) phases. The crystal structures of MIL-53(Al), originally determined by powder XRD data, are therefore validated by ^{17}O SSNMR data. The enhanced CSA effect at ultrahigh field of 35.2 T allows us to extract the ^{17}O CSA parameters. This work clearly demonstrates that ^{17}O SSNMR at very high magnetic fields is sensitive to the phase transitions in MOFs. Fine information on both MOF structure and host–guest interaction in MIL-53 systems is obtained from ^{17}O NMR spectra at 35.2 T owing to the very high spectral resolution and sensitivity achieved at this field. Such information is complementary to that those obtained from the ^{1}H, ^{13}C, and ^{27}Al SSNMR spectroscopy. The ability to completely resolve multiple chemically and, more importantly, crystallographically inequivalent oxygen sites in MOFs, as described in this work, greatly increases the potential for using NMR crystallography to determine the structures of new MOFs and refine the crystal structures of existing MOFs.

ACKNOWLEDGEMENTS

Jun Xu thanks the financial support from the National Natural Science Foundation of China (Project 21904071

and 22071115) and the Open Funds (KF1818) of the State Key Laboratory of Fine Chemicals. Yining Huang thanks the Natural Science and Engineering Research Council (NSERC) of Canada for a Discovery Grant. A portion of this work was performed at the NHMFL, which is supported by NSF DMR-1644779 and the State of Florida. In addition, development of the SCH magnet and NMR instrumentation was supported by the NSF (DMR-1039938 and DMR-0603042) and NIH (BTRR 1P41 GM122698). NMR spectroscopic calculations were performed by using HPC resources from GENCI-IDRIS (Grant 097535). We thank Dr V.V. Terskikh (University of Ottawa) for his assistance in acquiring 3QMAS spectrum at 21.1 T. Access to the 21.1 T NMR spectrometer was provided by the National Ultrahigh-Field NMR Facility for Solids (Ottawa, Canada), managed by University of Ottawa (http://nmr900.ca).

ORCID

Vinicius Martins https://orcid.org/0000-0002-5940-7038
Jun Xu https://orcid.org/0000-0003-3507-0159
Zhehong Gan https://orcid.org/0000-0002-9855-5113
Christel Gervais https://orcid.org/0000-0001-7450-1738
Christian Bonhomme https://orcid.org/0000-0003-0802-6961
Yining Huang https://orcid.org/0000-0001-9265-5896

REFERENCES

[1] a) H.-C. Zhou, J. R. Long, O. M. Yaghi, *Chem. Rev.* **2012**, *112*, 673. b) H. Furukawa, K. E. Cordova, M. O'Keeffe, O. M. Yaghi, *Science* **2013**, *341*, 1230444.

[2] a) A. Schneemann, V. Bon, I. Schwedler, I. Senkovska, S. Kaskel, R. A. Fischer, *Chem. Soc. Rev.* **2014**, *43*, 6062. b) Z. Chang, D.-H. Yang, J. Xu, T.-L. Hu, X.-H. Bu, *Adv. Mater.* **2015**, *27*, 5432.

[3] T. Loiseau, C. Serre, C. Huguenard, G. Fink, F. Taulelle, M. Henry, T. Bataille, G. Férey, *Chem. – Eur. J.* **2004**, *10*, 1373.

[4] G. Ortiz, G. Chaplais, J.-L. Paillaud, H. Nouali, J. Patarin, J. Raya, C. Marichal, *J. Phys. Chem. C* **2014**, *118*, 22021.

[5] a) R. Giovine, C. Volkringer, J. Trebosc, J.-P. Amoureux, T. Loiseau, O. Lafon, F. Pourpoint, *Acta Crystallogr. C* **2017**, *73*, 176. b) C. Paula, D. Wisser, M. Rangus, W. Schwieger, M. Hovestadt, M. Kriesten, K. Vanatalu, A. Oss, M.-L. Org, A. Samoson, M. Hartmann, *J. Phys. Chem. C* **2020**, *124*, 19136. c) C. Lieder, S. Opelt, M. Dyballa, H. Henning, E. Klemm, M. Hunger, *J. Phys. Chem. C* **2010**, *114*, 16596. d) Y. Jiang, J. Huang, S. Marx, W. Kleist, M. Hunger, A. Baiker, *J. Phys. Chem. Lett.* **2010**, *1*, 2886. e) B. Ibrahim, B. E. G. Lucier, J. Xu, P. He, Y. Huang, *Can. J. Chem.* **2015**, *93*, 960. f) A. E. Khudozhitkov, H. Jobic, D. Freude, J. Haase, D. I. Kolokolov, A. G. Stepanov, *J. Phys. Chem. C* **2016**, *120*, 21704. g) A. E. Khudozhitkov, S. S. Arzumanov, D. I. Kolokolov, A. G. Stepanov, *Microporous Mesoporous Mater.* **2020**, *300*, 110155. h) S. Li, J. Li, J. Tang, F. Deng, *Solid State Nucl. Magn. Reson.* **2018**, *90*, 1. i) M.-A. Springuel-Huet, A. Nossov, Z. Adem, F. Guenneau, C. Volkringer, T. Loiseau, G. Férey, A. Gédéon, *J. Am. Chem. Soc.* **2010**, *132*, 11599. j) T. K. Trung, P. Trens, N. Tanchoux, S. Bourrelly, P. L. Llewellyn, S. Loera-Serna, C. Serre, T. Loiseau, F. Fajula, G. Férey, *J. Am. Chem. Soc.* **2008**, *130*, 16926. k) L. Hamon, C. Serre, T. Devic, T. Loiseau, F. Millange, G. Férey, G. D. Weireld, *J. Am. Chem. Soc.* **2009**, *131*, 8775. l) A. Boutin, F.-X. Coudert, M.-A. Springuel-Huet, A. V. Neimark, G. Férey, A. H. Fuchs, *J. Phys. Chem. C* **2010**, *114*, 22237. m) F.-X. Coudert, M. Jeffroy, A. H. Fuchs, A. Boutin, C. Mellot-Draznieks, *J. Am. Chem. Soc.* **2008**, *130*, 14294. n) J. Y. Kim, J. Park, J. Ha, M. Jung, D. Wallacher, A. Franz, R. Balderas-Xicohténcatl, M. Hirscher, S. G. Kang, J. T. Park, I. H. Oh, H. R. Moon, H. Oh, *J. Am. Chem. Soc.* **2020**, *142*, 13278.

[6] a) L. Alaerts, M. Maes, L. Giebeler, P. A. Jacobs, J. A. Martens, J. F. M. Denayer, C. E. A. Kirschhock, D. E. De Vos, *J. Am. Chem. Soc.* **2008**, *130*, 14170. b) V. Finsy, C. E. A. Kirschhock, G. Vedts, M. Maes, L. Alaerts, D. E. De Vos, G. V. Baron, J. F. M. Denayer, *Chem. – Eur. J.* **2009**, *15*, 7724. c) W. De Malsche, S. Van der Perre, S. Silverans, M. Maes, D. E. De Vos, F. Lynen, J. F. M. Denayer, *Microporous Mesoporous Mater.* **2012**, *162*, 1.

[7] a) K. J. D. MacKenzie, M. E. Smith, *Multinuclear Solid-State NMR of Inorganic Materials*, Pergamon, Oxford; New York **2002**. b) A. I. Freytag, A. D. Pauric, S. A. Krachkovskiy, G. R. Goward, *J. Am. Chem. Soc.* **2019**, *141*, 13758.

[8] a) S. E. Ashbrook, M. E. Smith, *Chem. Soc. Rev.* **2006**, *35*, 718. b) G. Wu, *Prog. Nucl. Magn. Reson. Spectrosc.* **2019**, *114-115*, 135. c) K. Yamada, *Annu. Rep. NMR Spectrosc.* **2010**, *70*, 115. d) F. Castiglione, A. Mele, G. Raos, *Annu. Rep. NMR Spectrosc.* **2015**, *85*, 143. e) L. Buannic, F. Blanc, D. S. Middlemiss, C. P. Grey, *J. Am. Chem. Soc.* **2012**, *134*, 14483. f) T. M. Alam, M. Nyman, B. R. Cherry, J. M. Segall, L. E. Lybarger, *J. Am. Chem. Soc.* **2004**, *126*, 5610. g) S. T. Holmes, R. W. Schurko, *J. Phys. Chem. C* **2018**, *122*, 1809. h) C. P. Romao, F. A. Perras, U. Werner-Zwanziger, J. A. Lussier, K. J. Miller, C. M. Calahoo, J. W. Zwanziger, M. Bieringer, B. A. Marinkovic, D. L. Bryce, M. A. White, *Chem. Mater.* **2015**, *27*, 2633. i) Y. Champouret, Y. Coppel, M. L. Kahn, *J. Am. Chem. Soc.* **2016**, *138*, 16322.

[9] R. K. Harris, E. D. Becker, S. M. Cabral De Menezes, R. Goodfellow, P. Granger, *Pure Appl. Chem.* **2001**, *73*, 1795.

[10] a) J. M. Griffin, L. Clark, V. R. Seymour, D. W. Aldous, D. M. Dawson, D. Iuga, R. E. Morris, S. E. Ashbrook, *Chem. Sci.* **2012**, *3*, 2293. b) M. Wang, X.-P. Wu, S. Zheng, L. Zhao, L. Li, L. Shen, Y. Gao, N. Xue, X. Guo, W. Huang, Z. Gan, F. Blanc, Z. Yu, X. Ke, W. Ding, X.-Q. Gong, C. P. Grey, L. Peng, *Sci. Adv.* **2015**, *1*, e1400133. c) T.-X. Métro, C. Gervais, A. Martinez, C. Bonhomme, D. Laurencin, *Angew. Chem., Int. Ed.* **2017**, *56*, 6803. d) P. He, J. Xu, V. V. Terskikh, A. Sutrisno, H.-Y. Nie, Y. Huang, *J. Phys. Chem. C* **2013**, *117*, 16953. e) G. P. M. Bignami, Z. H. Davis, D. M. Dawson, S. A. Morris, S. E. Russell, D. McKay, R. E. Parke, D. Iuga, R. E. Morris, S. E. Ashbrook, *Chem. Sci.* **2018**, *9*, 850. f) C. M. Rice, Z. H. Davis, D. McKay, G. P. M. Bignami, R. G. Chitac, D. M. Dawson, R. E. Morris, S. E. Ashbrook, *Phys. Chem. Chem. Phys.* **2020**, *22*, 14514.

[11] V. Martins, J. Xu, X. Wang, K. Chen, I. Hung, Z. Gan, C. Gervais, C. Bonhomme, S. Jiang, A. Zheng, B. E. G. Lucier, Y. Huang, *J. Am. Chem. Soc.* **2020**, *142*, 14877.

[12] a) E. G. Keeler, V. K. Michaelis, M. T. Colvin, I. Hung, P. L. Gor'kov, T. A. Cross, Z. Gan, R. G. Griffin, *J. Am. Chem. Soc.*

2017, *139*, 17953. b) Z. Gan, I. Hung, X. Wang, J. Paulino, G. Wu, I. M. Litvak, P. L. Gor'kov, W. W. Brey, P. Lendi, J. L. Schiano, M. D. Bird, I. R. Dixon, J. Toth, G. S. Boebinger, T. A. Cross, *J. Magn. Reson.* **2017**, *284*, 125. c) C. Bonhomme, X. Wang, I. Hung, Z. Gan, C. Gervais, C. Sassoye, J. Rimsza, J. Du, M. E. Smith, J. V. Hanna, S. Sarda, P. Gras, C. Combes, D. Laurencin, *Chem. Commun.* **2018**, *54*, 9591. d) E. G. Keeler, V. K. Michaelis, C. B. Wilson, I. Hung, X. Wang, Z. Gan, R. G. Griffin, *J. Phys. Chem. B* **2019**, *123*, 3061. e) Q. Wang, W. Li, I. Hung, F. Mentink-Vigier, X. Wang, G. Qi, X. Wang, Z. Gan, J. Xu, F. Deng, *Nat. Commun.* **2020**, *11*, 3620.

[13] I. Hung, J. Trébosc, G. L. Hoatson, R. L. Vold, J.-P. Amoureux, Z. Gan, *J. Magn. Reson.* **2009**, *201*, 81.

[14] D. Massiot, F. Fayon, M. Capron, I. King, S. Le Calve, B. Alonso, J.-O. Durand, B. Bujoli, Z. Gan, G. Hoatson, *Magn. Reson. Chem.* **2002**, *40*, 70.

[15] P. P. Man, in *Encyclopedia of Analytical Chemistry*, (Ed: R. A. Meyers), John Wiley & Sons Ltd, Chichester **2000** 12224.

[16] G. Kresse, J. Hafner, *Phys. Rev. B* **1994**, *49*, 14251.

[17] P. Giannozzi, S. Baroni, N. Bonini, M. Calandra, R. Car, C. Cavazzoni, D. Ceresoli, G. L. Chiarotti, M. Cococcioni, I. Dabo, A. Dal Corso, S. de Gironcoli, S. Fabris, G. Fratesi, R. Gebauer, U. Gerstmann, C. Gougoussis, A. Kokalj, M. Lazzeri, L. Martin-Samos, N. Marzari, F. Mauri, R. Mazzarello, S. Paolini, A. Pasquarello, L. Paulatto, C. Sbraccia, S. Scandolo, G. Sclauzero, A. P. Seitsonen, A. Smogunov, P. Umari, R. M. Wentzcovitch, *J. Phys.: Condens. Matter* **2009**, *21*, 395502.

[18] C. J. Pickard, F. Mauri, *Phys. Rev. B* **2001**, *63*, 245101.

[19] N. Troullier, J. L. Martins, *Phys. Rev. B* **1991**, *43*, 1993.

[20] L. Kleinman, D. M. Bylander, *Phys. Rev. Lett.* **1982**, *48*, 1425.

[21] L. Frydman, J. S. Harwood, *J. Am. Chem. Soc.* **1995**, *117*, 5367.

[22] J.-P. Amoureux, C. Huguenard, F. Engelke, F. Taulelle, *Chem. Phys. Lett.* **2002**, *356*, 497.

[23] a) T. Charpentier, *Solid State Nucl. Magn. Reson.* **2011**, *40*, 1. b) C. Bonhomme, C. Gervais, F. Babonneau, C. Coelho, F. Pourpoint, T. Azaïs, S. E. Ashbrook, J. M. Griffin, J. R. Yates, F. Mauri, C. J. Pickard, *Chem. Rev.* **2012**, *112*, 5733. c) X. Kong, V. V. Terskikh, R. L. Khade, L. Yang, A. Rorick, Y. Zhang, P. He, Y. Huang, G. Wu, *Angew. Chem., Int. Ed.* **2015**, *54*, 4753. d) E. Pavón, F. J. Osuna, M. D. Alba, L. Delevoye, *Solid State Nucl. Magn. Reson.* **2019**, *100*, 45. e)A. Pedone, E. Gambuzzi, M. C. Menziani, *J. Phys. Chem. C* **2012**, *116*, 14599.

SUPPORTING INFORMATION

Additional supporting information may be found online in the Supporting Information section at the end of this article.

How to cite this article: Martins V, Xu J, Hung I, et al. ^{17}O solid-state NMR at ultrahigh magnetic field of 35.2 T: Resolution of inequivalent oxygen sites in different phases of MOF MIL-53(Al). *Magn Reson Chem*. 2021;1–11. https://doi.org/10.1002/mrc.5122